

# Estimating 3D Human Pose on a Configurable Bed from a Single Pressure Image

Henry M. Clever\*, Ariel Kapusta, Daehyung Park, Zackory Erickson, Yash Chitalia, Charles C. Kemp

**Abstract**—Robots have the potential to assist people in bed, such as in healthcare settings, yet bedding materials like sheets and blankets can make observation of the human body difficult for robots. A pressure-sensing mat on a bed can provide pressure images that are relatively insensitive to bedding materials. However, prior work on estimating human pose from pressure images has been restricted to 2D pose estimates and flat beds. In this work, we present two convolutional neural networks to estimate the 3D joint positions of a person in a configurable bed from a single pressure image. The first network directly outputs 3D joint positions, while the second outputs a kinematic model that includes estimated joint angles and limb lengths. We evaluated our networks on data from 17 human participants with two bed configurations: *supine* and *seated*. Our networks achieved a mean joint position error of 77 mm when tested with data from people outside the training set, outperforming several baselines. We also present a simple mechanical model that provides insight into ambiguity associated with limbs raised off of the pressure mat, and demonstrate that Monte Carlo dropout can be used to estimate pose confidence in these situations. Finally, we provide a demonstration in which a mobile manipulator uses our network’s estimated kinematic model to reach a location on a person’s body in spite of the person being seated in a bed and covered by a blanket.

## I. INTRODUCTION

Various circumstances, such as illness, injury, or longterm disabilities can result in people receiving assistance in bed. Previous work has shown how robots can provide assistance with ADLs [1]–[3], but providing assistance to a person in bed can be challenging. Estimating the pose of a person’s body could enable robots to provide better assistance. Typical methods of body pose estimation use line-of-sight sensors, such as RGB cameras, which can have difficulties when the body is occluded by blankets, loose clothing, medical equipment, over-bed trays and other common items in healthcare settings, such as hospitals. A pressure-sensing mat on the bed can allow for estimation of the body’s pose in a manner that is less sensitive to bedding materials and surrounding objects [2], [4]–[6]. In this work, we present a method for estimating the 3D joint positions with a measure of confidence in each estimated position for a person in a configurable bed using a pressure-sensing mat.

In prior work, we used a pressure mat on a configurable bed to estimate the location of a person’s head for positioning a rigid geometric model of a human body [2]. In this paper, we propose and compare two convolutional neural network (ConvNet) architectures to learn a mapping from a pressure

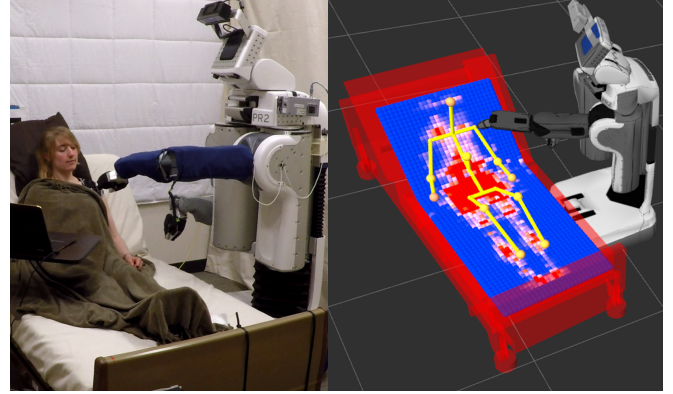


Fig. 1. We demonstrate how an assistive robot could use our 3D human pose estimation method. A PR2 robot uses our method’s body pose estimation to reach to a person’s shoulder.

image and bed configuration to ten 3D human joint positions: the head, neck, elbows, wrists, knees, and ankles. We trained and tested our methods on a 17-human participant dataset with over 28,000 pressure images. Our first method directly regresses to the 3D ground truth labels ( $x$ ,  $y$ ,  $z$ ). Our second method embeds a 17-joint kinematics skeleton model of the human to the last layer of the ConvNet to enforce constraints on bone lengths and joint angles. The latter provides a more complete pose representation with unlabeled joints and latent space joint angle estimates. We train the kinematics ConvNet end-to-end, backpropagating from 3D Euclidean error through the kinematics model. We compare constant skeleton link length and regression to an approximated link length that adjusts the model for anatomical variance.

Our configurable bed, introduced previously as Autobed [2], [7], features adjustable height, leg rest angle, and head rest angle. Autobed can sense its own state, sense the pressure distribution of the person on the bed, and communicate with other devices. In this work, we estimate the human joint positions in two Autobed configurations by adjusting the bed’s head rest: *supine* ( $0^\circ$  flat) and *seated* ( $60^\circ$  incline).

Lack of contact by limbs or other body parts presents a challenging issue for the pressure image modality. In this work, we consider common poses where this issue arises, such as an arm raised in the air resembling a double inverted pendulum. Among other poses, this case demonstrates where the measured pressure image can be similar for different configurations of the arm. In such a case, the pressure data may be insufficient to confidently estimate the pose of the arm. An estimate of confidence or model uncertainty can be valuable, for example to allow an assistive robot to reject low-confidence estimates by removing them from a list of

H. Clever, A. Kapusta, D. Park, Y. Chitalia, Z. Erickson and C. Kemp are with the Healthcare Robotics Lab, Institute for Robotics and Intelligent Machines, Georgia Institute of Technology,

\*H. Clever is the corresponding author. henryclever@gatech.edu

potential goals in task plan execution. To estimate model uncertainty, we use Monte Carlo dropout, a method proposed by Gal and Ghahmarani [8]. Using this method, we perform a number of stochastic forward passes through the ConvNet during test time and compute the output joint position estimate and confidence from the moments of the output distribution.

## II. RELATED WORK

3D pose estimation methods can be classified as one of three strategies: *generative* (model-based), which imposes a model from prior information, *discriminative* (model-free), which learns a mapping between output labels and input images, and *hybrid*, which fuses the two [9].

### A. Human Body Pose Estimation

1) *More Classical Data-Driven Methods*: Discriminative approaches, such as ridge regressors, have been applied with success to 3D pose estimation in [10]–[12]. Okada and Soatto [10] use kernel ridge regression (KRR) as well as linear ridge regression (LRR). Ionescu et al. [11] compare K-Nearest Neighbors (KNN) and ridge regression on the Human3.6M dataset.

2) *2D Pose Estimation with ConvNets*: With the advent of high quality, labeled synchronous datasets such as Human3.6M [11], many researchers have taken discriminative approaches such as end-to-end training of ConvNets [13]–[16]. Since Toshev and Szegedy [13] and Thompson et al. [14] first applied ConvNets to 2D pose estimation, many researchers have explored various ConvNet architectures using RGB cameras. Two common ConvNet approaches include direct regression to joint labels [13], [17] and regression to discretized confidence maps [14], [15], [18].

3) *3D Pose Estimation with ConvNets from Monocular RGB*: Several researchers have used confidence maps for 3D pose estimation from a monocular RGB cameras [15], [19], [20]. However, the high dimensional output space of confidence maps can make real-time pose estimation difficult. Li and Chan [17] use rapid direct regression to 3D Cartesian joint positions; we implement a similar architecture because real-time estimation is important to our planned application. Zhou, Sun et al. [16] take a hybrid approach, by training a ConvNet end-to-end and enforcing anthropomorphic constraints with an embedded human skeleton kinematics model with constant link lengths. In contrast, we introduce a variant of their architecture that regresses to variable link lengths to allow the model to adapt to differently sized people.

Work on pose estimation in the context of entertainment and human-computer interaction often estimates the body with respect to a local reference frame [11], [17]. To find the poses in an external or global reference frame (e.g., the camera's frame), they estimate the transformation from the external frame to the local frame. In our method we estimate the body pose directly in an external reference frame, specifically located at the bottom left corner of the pressure sensing mat.

4) *Pose Estimation from Pressure Images*: Prior pressure-image-based pose estimation works have taken model-based approaches, fitting 2D kinematic models to the pressure images [5], [21], [22]. We also use a kinematic model, but take a hybrid approach by embedding the model into a ConvNet.

We show that our data-driven methods can estimate body pose in 3D for nontrivial configurations of the body. We consider more challenging situations where the bed and human are configured in a seated posture, and when limbs (1) extend off the side of the bed and (2) extend up in the air.

5) *Posture Classification from Pressure Images*: A few researchers have also looked at posture classification from pressure images [6], [23], [24]. Posture classification is a different problem from 3D body pose estimation, but it can be used in a complementary way, e.g. by providing a prior on the model used for pose estimation.

### B. Monte Carlo Dropout in ConvNets

We use Monte Carlo dropout to measure network uncertainty, a method introduced by Gal and Ghahramani [8]. Monte Carlo dropout has been applied to measure uncertainty for camera relocalization [25] and semantic segmentation [26]. We use this method to estimate pose and provide a measure of confidence.

## III. METHOD

Our ConvNets learn a function  $f(\mathcal{P}, \theta_B)$  that estimates pose parameters of a person lying in a robotic bed, given a specified bed configuration  $\theta_B$  and a 2D pressure image  $\mathcal{P}$  from a pressure mat.

### A. ConvNet Architecture

We explore two ConvNet architectures shown in Fig. 2. Our network includes four 2D convolutional layers with 64 output channels for the first two layers and 128 channels for the last two layers. The layers mostly have  $3 \times 3$  filters, with a ReLU activation and a dropout of 10% applied after each layer. We apply max pooling, and the network ends with a linear fully connected layer.

To estimate a person's joint pose, we construct an input tensor for the ConvNet comprised of three channels, i.e.  $\{\mathcal{P}, E, B\} \in \mathbb{R}^{128 \times 54 \times 3}$ . Raw data from the pressure sensing mat is recorded as a  $(64 \times 27)$ -dimensional image, which we upsample by a factor of two, i.e.  $\mathcal{P} \in \mathbb{R}^{128 \times 54}$ . In addition to a pressure map, we also provide the ConvNet with an edge detection channel,  $E \in \mathbb{R}^{128 \times 54}$ , which is computed as a Sobel filter over both the horizontal and vertical directions of the upsampled image. Empirically, we found this edge detection input channel improved pose estimation performance. In order to estimate human pose at different configurations of the bed (e.g. sitting versus lying down), we compute a third input channel,  $B \in \mathbb{R}^{128 \times 54}$ , which depicts the bed configuration. Specifically, each element in the matrix  $B$  depicts the vertical height of the corresponding taxel on the pressure mat. When the bed frame is flat, i.e.  $\theta_B = 0$ , then  $B$  is simply the zero matrix.

### B. Direct Joint Regression

The first proposed ConvNet architecture outputs an estimate of the motion capture labeled global 3D joint positions  $\{\hat{s}_1, \dots, \hat{s}_N\}$ , where each  $\hat{s}_j \in \mathbb{R}^3$  represents a 3D position estimate for joint  $j$ . The direct ConvNet regresses directly to 3D ground truth label positions in the last fully connected layer of the network. We use an  $L_1$  norm loss function on the joint Euclidean error.

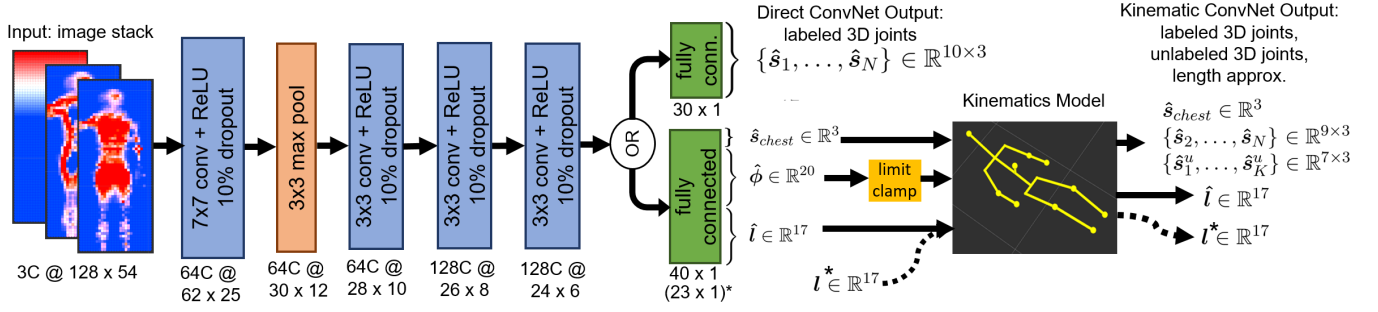


Fig. 2. Two ConvNet architectures. The *Direct ConvNet* directly regresses to ten motion capture labeled global joint positions. The *Kinematic ConvNet* embeds a kinematics skeleton model into the last fully connected network layer, parameterized in the latent space by a root joint global position, joint angles, and skeleton link lengths. The *Kinematic ConvNet* also outputs unlabeled joint position estimates. We explore architectures with both variable link length (shown) and constant link length (dashed arrows, defined by \*.)

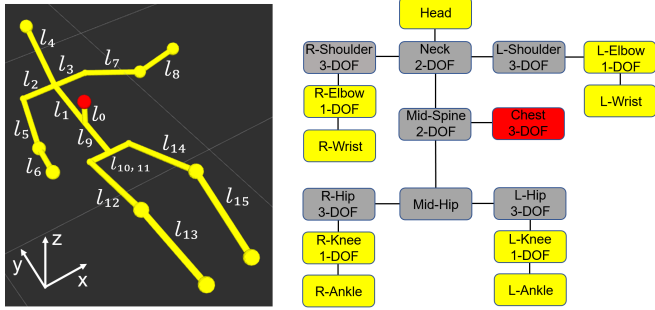


Fig. 3. Kinematics Model Parameters. The root joint  $s_{chest}$  is specified in red. Yellow boxes represent the remaining motion capture labeled joints  $\{\hat{s}_2, \dots, \hat{s}_N\}$ . Grey boxes represent unlabeled joints  $\{\hat{s}_1^u, \dots, \hat{s}_K^u\}$ , where the kinematic model adjusts to an approximate fit.

### C. Deep Kinematic Embedding

We embed a human skeleton kinematics model into the last fully connected network layer to enforce geometric and anthropomorphic constraints. This creates an extra network layer where labeled joint estimates  $\{\hat{s}_1, \dots, \hat{s}_N\}$  and unlabeled joint estimates  $\{\hat{s}_1^u, \dots, \hat{s}_K^u\}$  are solved through forward kinematics equations depending on root joint position  $\hat{s}_1$ , latent space joint angles  $\hat{\phi}$  and an estimate of skeleton link length approximations  $\hat{l}$ . We use  $\hat{s}_1 = \hat{s}_{chest}$  as the root joint. We incorporate skeleton link lengths  $l$  into the loss function by pre-computing an approximation to the ground truth. While the kinematics functions are relative to a root joint, we learn root joint global position  $s_{chest}$  to put our output in global space. We apply the  $L_1$  norm to our kinematics ConvNet loss function shown below:

$$\text{Loss}_{\text{kin.}} = \|s_1 - \hat{s}_1\| + \alpha \sum_{j=2}^N \|s_j - \hat{s}_j\| + \beta \|l - \hat{l}\| \quad (1)$$

where  $\alpha$  and  $\beta$  are weighting factors. We compare two variants of this loss function: The *variable link length* ConvNet is as described, while for the *constant link length* ConvNet we set  $\beta = 0$  and use a constant  $l^*$  input to the kinematics model. We compute  $l^*$  as the average of the approximations  $l$ .

1) *Human Kinematics Model*: We represent the human body with a model similar to that used in other works [11], [16], [17], [27], with 17 joints to cover major links down to the wrists and ankles. We ignore minor links and joints. To train the networks that have link lengths as an output,

we require ground truths for comparison. Some ground truth link lengths may be calculated directly from the dataset's labels, for example when motion capture gives the location of both ends of the link. We approximate the link lengths for links that are under-constrained in the dataset for the skeleton model. The link lengths are an output of our network as a  $l \in \mathbb{R}^{17}$  vector. We ignore unlabeled joints in the loss function.

The mid-spine is found by a vertical offset from the chest marker to compensate for the distance between marker placement atop the chest and the modeled bending point of the spine. We do not make offset corrections with other joints; these are more challenging than the chest and the effects are less noticeable.

2) *Angular Latent Space*: We define 20 angular degrees of freedom consisting of 3-DOF shoulders and hips, 1-DOF elbow and knee joints, a 2-DOF neck joint, and a 2-DOF spine joint. Fig 3 (b) shows this parameterization corresponding to labeled and unlabeled joints. For the spine of the model to better match the spine of a person seated in bed, we used two revolute joints about the  $x$ -axis. We use PyTorch [28], a deep learning library with tensor algebra and automatic differentiation. We manually encoded the forward kinematics for the skeleton kinematic model. The network uses stochastic gradient descent during backpropagation to find inverse kinematics (IK) solutions.

### D. Uncertainty: Monte Carlo Dropout

To estimate both joint position and model uncertainty simultaneously, we apply Monte Carlo dropout from Gal and Ghahramani [8]. Monte Carlo dropout is the process of performing  $V$  forward passes through the network with dropout enabled. This results in  $V$  output vectors which may differ slightly due to the stochastic dropout of data during each forward pass. We can compute an estimated output as the average of all  $V$  outputs, corresponding to the first moment of the predictive distribution within the network. Similarly, the model's uncertainty corresponds to the second moment of the distribution, which we can compute as the variance of all  $V$  forward passes.

## IV. DATASET: 17 HUMAN PARTICIPANTS

We recorded a motion capture labeled dataset with over 28,000 pressure images from 17 different human participants.

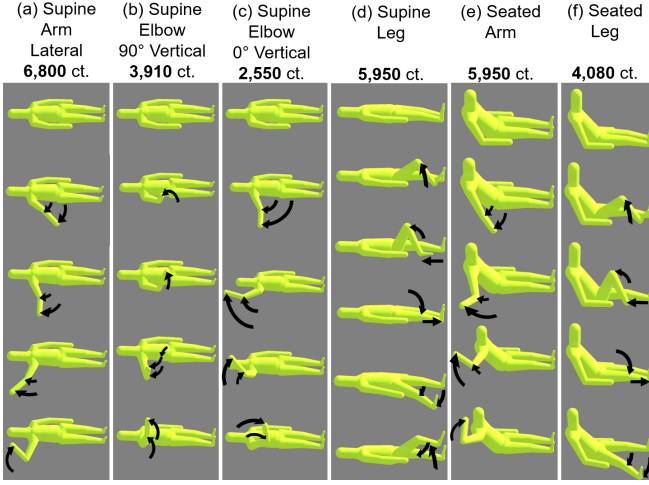


Fig. 4. Range of paths traversed by participants during training. Equivalent paths were traversed by the left limbs. Count represents both left and right data across 17 participants.

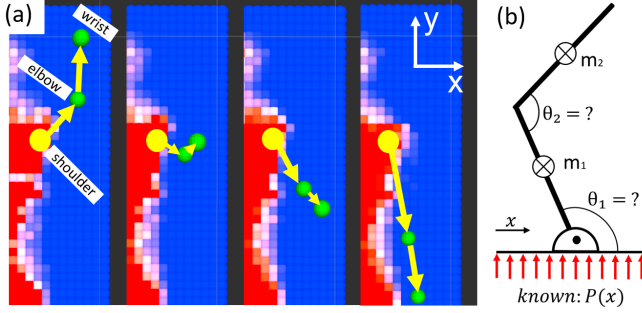


Fig. 5. (a) Crossover of the shoulder from the *supine elbow 0 vertical* traversal, both joints envisioned as 2-DOF inverted pendulum. Green dots represent left elbow and wrist ground truth markers projected in 2D, yellow dot and arrows indicate approximate shoulder and limb positions. (b) Model of 2-DOF inverted pendulum showing static indeterminacy. Known pressure distribution  $P(x)$  is insufficient to solve  $\theta_1, \theta_2$ .

We conducted this study with approval from the Georgia Institute of Technology Institutional Review Board (IRB), and obtained informed consent from all participants. We recruited 11 male and 6 female participants aged 19-32, who ranged 1.57-1.83 m in height and 45-94 kg in weight. We fitted participants with motion capture markers at the wrists, elbows, knees, ankles, head, and chest. We used a commercially available  $64 \times 27$  pressure mat from Boditrak sampled at 7 Hz. We asked each participant to move their limbs in 6 patterns, 4 while supine and 2 while seated, to represent some common poses in a configurable bed. The movement paths are shown in Fig. 4. We instructed participants to keep their torso static during limb movements.

#### A. Sensory Limitations

Raising a limb off the pressure mat can lead to a loss of information as the mat can only sense pressure during contact. A similar loss of information can be seen when the limbs stick off the edge of the pressure mat. Consider the movement shown in Fig. 4 (a) and an example of the pressure images associated with such a movement in Fig. 5 (a)-upper. Here, the pressure images appear nearly identical while the elbow and wrist positions change substantially. To better understand

what is physically causing this phenomena, we can model the arm as a double inverted pendulum, shown in Fig. 5 (b). Here, the pendulum angles  $\theta_1$  and  $\theta_2$  are statically indeterminate given an underlying pressure distribution, until part of the arm touches the mat.

Another challenge is pressure mat resolution. The taxels under the shoulders, back, and hips often saturate. A pressure sensing mat with higher spatial resolution, accuracy, and pressure range may result in less ambiguity. We note that the inverted pendulum model could be resolved for capsule limbs with the base joint sunk into the mat, but we find that in practice with the limitations in the mat's sensing, the pressure images are ambiguous.

### V. EVALUATION

At each training epoch for the ConvNets, we selected images such that each participant would be equally represented in both the training and test sets. We augmented the original dataset by the following to increase training data diversity:

- *Flipping*. Flipped across the longitudinal axis with probability  $P = 0.5$ .
- *Shifting*. Shifted by an additive factor  $sh \sim \mathcal{N}(\mu = 0\text{cm}, \sigma = 2.86\text{cm})$ .
- *Scaling*. Scaled by a multiplicative factor  $sc \sim \mathcal{N}(\mu = 1, \sigma = 0.06)$ .
- *Noise*. Added taxel-by-taxel noise to images by an additive factor  $\mathcal{N}(\mu = 0, \sigma = 1)$ . Clipped the noise at min pressure (0) and at the saturated pressure value (100).

We chose these to improve the network's ability to generalize to new people and positions of the person in bed. We did not shift the seated data longitudinally or scale it because of the warped spatial representation.

We trained six data-driven models: three baseline supervised learning algorithms and the three proposed ConvNet architectures. We performed leave-one-participant-out cross validation on 10 participants (6M, 4F).

#### A. Baseline Comparisons

We implemented three baseline methods to compare our ConvNets against: K-nearest neighbors (KNN), Linear Ridge Regression (LRR), and Kernel Ridge Regression (KRR). For all baseline methods, we used histogram of oriented gradients (HOG) features [29] on  $2 \times$  upsampled pressure images. We applied flipping, shifting, and noise augmentation methods. We did not use scaling, as it worsened performance.

1) *K-Nearest Neighbors*: We implemented a K-nearest neighbors (KNN) regression baseline using Euclidean distance on the HOG features to select neighbors, as [11] did. We selected  $k = 10$  for improved performance.

2) *Ridge Regression*: We implemented two ridge-regression-based baselines. Related work using these methods are described in Section II. We trained linear ridge regression (LRR) models with a regularization factor of  $\alpha = 0.7$ . We also train Kernel Ridge Regression (KRR) models with a radial basis function (RBF) kernel and  $\alpha = 0.4$ . We manually selected these values of  $\alpha$  for both LRR and KRR.



### B. Implementation Details of Proposed ConvNets

During testing, we estimate the joint positions with  $V = 25$  forward passes on the trained network with Monte Carlo dropout for each test image. For each joint, we report the mean of the forward passes as the estimated joint position. We use PyTorch and ADAM from [30] for gradient descent.

1) *Pre-trained ConvNet*: We created a pre-trained ConvNet that we use to initialize both Kinematic ConvNets, with regressed and constant link length. The pre-trained network used the kinematically embedded ConvNet and the loss function in Eq. 1, with  $\alpha = 0.5$  and  $\beta = 0.5$ . This network was trained for 10 epochs on the 7 network-design participants with a learning rate of 0.00002 and weight decay of 0.0005.

2) *Direct ConvNet*: We trained the network for 300 epochs directly on motion capture ground truth, using the sum of Euclidean error as the loss function. We used a learning rate of 0.00002 and a weight decay of 0.0005.

3) *Kinematic ConvNet, Constant Link Length*: We trained the network through the kinematically embedded ConvNet, used the loss function in Eq. 1, with  $\alpha = 0.5$  and  $\beta = 0$ . This value for  $\beta$  means the network would not regress to link length, leaving it constant. We initialized the network with the pre-trained ConvNet, but we separately initialized each link length as the average across all images in the fold's training set for each fold of cross validation.

4) *Kinematic ConvNet, Regress Link Length*: We trained the network through the kinematically embedded ConvNet, used the loss function in Eq. 1, with  $\alpha = 0.5$  and  $\beta = 0.5$ . Joint Cartesian positions and link lengths in the ground truth are represented on the same scale. We initialized with the pre-trained ConvNet.

### C. Measure of Uncertainty

Here we show an example where ambiguous pressure mat data has a high model uncertainty. We compare two leg abduction movements from the *supine leg* motion, shown in the bottom two columns of Fig. 4 (d). We sample 100 images per participant: half feature leg abduction contacting the pressure mat, and half with elevated leg abduction. For each pose, we use  $V = 25$  stochastic forward passes and compute the standard deviation of the Euclidean distance from the mean for abducting joints, including knees and feet. We compare this metric between elevated and in-contact motions.

## VI. RESULTS

In Table I, we present the mean per joint position error (MPJPE), a metric from literature to represent overall accuracy [11], [17]. Fig. 7 shows the per-joint position error across all trained models, separated into supine and seated postures. The error for the direct ConvNet and the kinematic ConvNet with length regression is significantly lower than the other methods. The results of knees and legs show that more distal limbs on the kinematic chain do not necessarily result in higher error. The wrists are both distal and light, and have higher error than the other joints. Fig. 6 shows the kinematics ConvNet with length regression adjusting for humans of different sizes and in different poses. Furthermore, we can

TABLE I: Global Joint Euclidean Error.

Method	MPJPE	MPJPE	MPJPE
	Supine (mm)	Seated (mm)	Overall (mm)
K-Nearest Neighbors	102.01	93.42	99.06
Linear Ridge Regression	117.01	114.76	116.24
Kernel Ridge Regression	99.25	97.10	98.51
Direct ConvNet	73.49	82.44	<b>76.56</b>
Kinematic ConvNet, avg. $\mathbf{l}$	99.74	99.70	99.72
Kinematic ConvNet, regr. $\mathbf{l}$	75.43	79.19	<b>76.72</b>

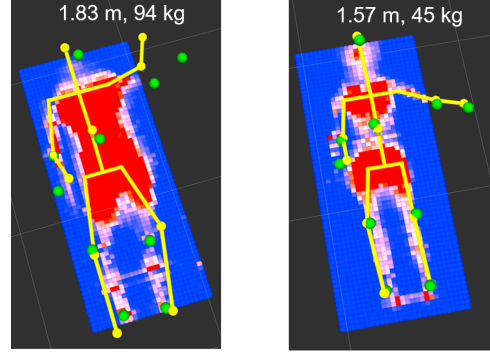


Fig. 6. Comparison of the heaviest and tallest participant with the lightest and shortest participant. Our kinematics ConvNet with link length regression appears to adjust for both sizes.

perform a pose estimate with uncertainty using  $V = 25$  stochastic forward passes in less than a half second.

### A. Measure of Uncertainty

We performed a t-test to compare uncertainty in elevated leg abduction and in-contact leg abduction. We compared each knee and ankle separately. We found that the standard deviation of the Euclidean distance from the mean of  $V = 25$  forward passes with Monte Carlo dropout is significantly higher for joints in the elevated position. Further, we note that variance in the latent angle parameters  $\theta$  compounds through the kinematic model, causing more distal joints in the kinematic chain to have higher uncertainty. This phenomena is further described in Fig. 8, which shows limbs removed from the mat that have a high variance.

## VII. DISCUSSION AND LIMITATIONS

### A. Network Architecture Considerations

While the results for the direct ConvNet architecture were marginally better than the kinematic ConvNet with variable lengths, the latter has other advantages. First, there can be value in getting a skeletal model from the network, providing a more complete set of parameters including 20 angular DOFs and a total of 17 joint positions. Second, unsurprisingly, requiring that outputs from the ConvNet satisfy kinematic constraints means that outputs will be constrained to plausible looking body poses. Without those constraints the ConvNet could produce unrealistic outputs.

### B. Data Augmentation Challenges

Data augmentation cannot easily account for person sliding up and down in a bed that is not flat. Vertical shifting augmentation for non-flat beds would not match the physical

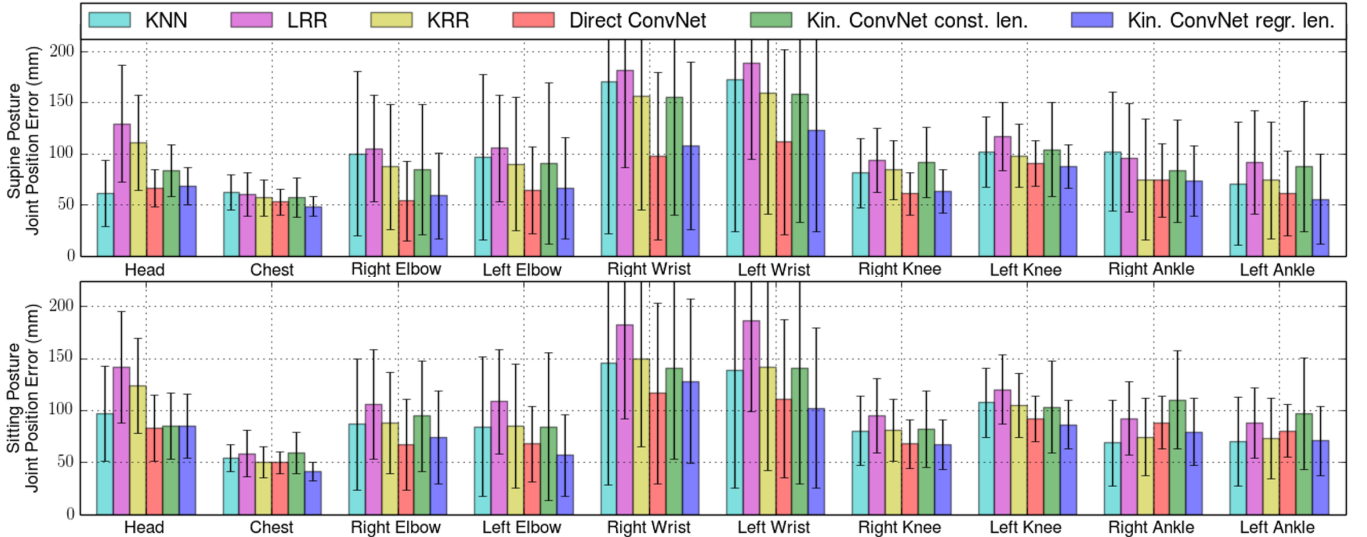


Fig. 7. Per-joint error mean and standard deviation for leave-one-participant-out cross validation over 10 participants for a sitting and a supine posture in bed. Lower is better. Our methods outperformed baseline methods.

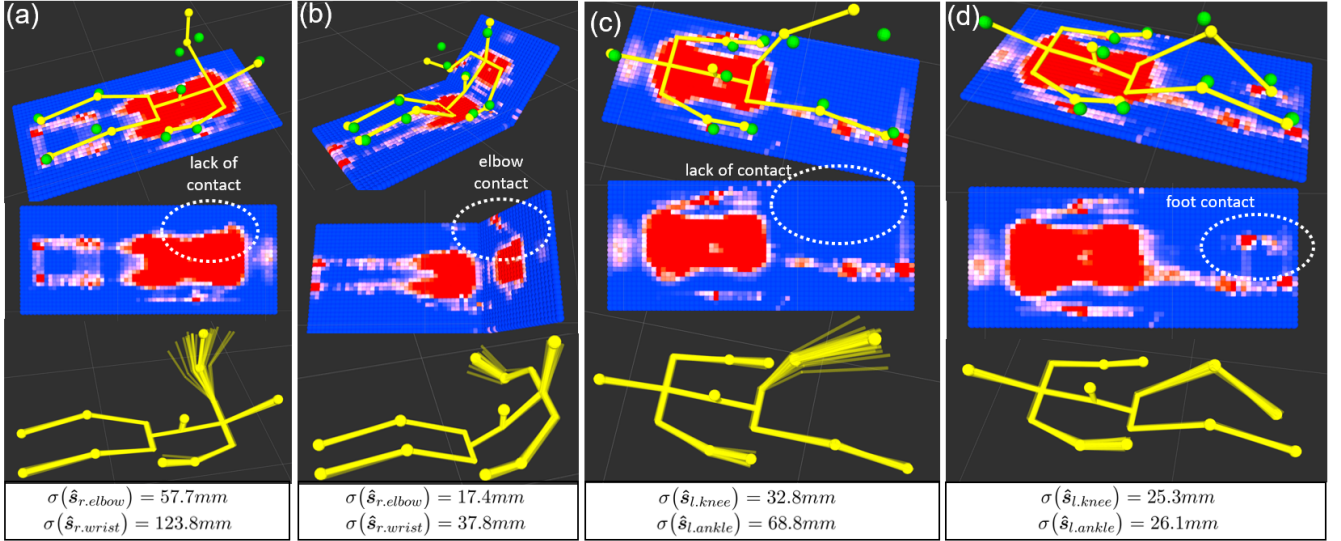


Fig. 8. Illustration of mean and standard deviation of kinematic ConvNet ( $l$  regression) output.  $V = 25$  forward passes with Monte Carlo dropout shown with thin translucent skeleton links. Spheres indicate joint position estimates. (a) Right arm thrust into the air. (b) Right forearm extending off the side of the pressure mat. (c) Left leg extended in the air and abducted. (d) Left knee extended in the air, left foot contacting pressure mat. Note: (c) and (d) show the same participant, others are different.

effects of shifting a person on the pressure mat. Augmentation by scaling also has problematic implications, because a much smaller or larger person may have a weight distribution that would not scale linearly at the bending point of the bed. Simulation might resolve these issues by simulating placing a weighted human model of variable shape and size placed anywhere on a simulated pressure mat, with many possibilities of bed configurations.

### C. Dataset Considerations

The posture and range of paths traversed by participants may not be representative of other common poses, and we expect our method to have limited success in generalizing to body poses not seen or rarely seen in the dataset. While a participant is moving their arm across a specified path, other joints remain nearly static, which over-represents poses

with the arms adjacent to the chest and legs straight. We found over-represented poses to generally have a lower uncertainty. Interestingly, with our current sampling and training strategy, over-representation and under-representation is based on the percentage representation in the dataset, not in absolute representation. Additional epochs of training or directly scaling the size of the dataset does not change these effects on uncertainty of pose representation. Our method could be improved by using weighting factors or sampling strategies to compensate for this effect.

In our evaluation, some limb poses occur in separate training images, but do not occur in the same training image. For example, we recorded one participant moving both arms and both legs simultaneously. Fig. 9 shows that our method has some ability to estimate these poses.

The skeleton model has offset error in addition to the

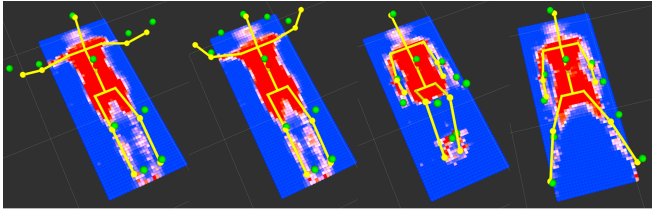


Fig. 9. Dual arm and dual leg traversals. While these are excluded from the training set, our methods can provide a reasonable pose estimate.

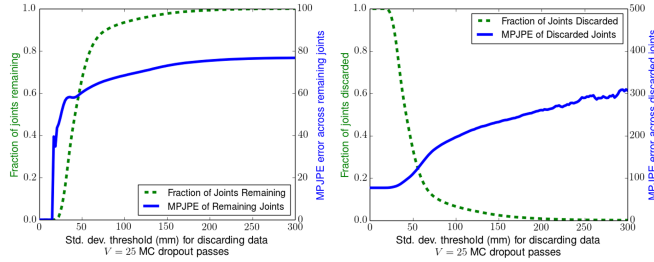


Fig. 10. Discarding joints with a higher uncertainty can decrease error, with a tradeoff to the number of joints remaining.

ground truth error reported. While we attempted to compensate for the chest marker offset, the other markers were more challenging. This may have caused some inaccuracy in the link length approximations.

#### D. Removal of High Variance Joints

Fig. 10 shows that joints with high uncertainty have a higher average error. Discarding these joint estimates can decrease the average error of the model. As an example application, a robot using our method’s estimated poses for task and motion planning might want to require low uncertainty before plan execution.

### VIII. DEMONSTRATION WITH PR2 ROBOT

We conducted a demonstration of how our method could inform an assistive robot trying to reach part a person’s body. We conducted this study with approval from the Georgia Institute of Technology IRB, and obtained informed consent from the participant. We recruited a single participant who used a laptop computer running a web interface from [3] to command a PR2 robot to move its end effector to their left knee and to their left shoulder. The robot’s goal was based on the estimated pose of the person’s body from our ConvNet with kinematic model regressing to link lengths. For the knee position, the participant raised their knee to the configuration shown in the 2nd image of Fig. 4 (f), and the participant was in the seated posture for both tasks. Using our 3D pose estimation method, the robot was able to autonomously reach near both locations. Fig 1 shows the robot reaching a shoulder goal while the participant is occluded by bedding.

### IX. CONCLUSION

In this work, we have shown that a pressure sensing mat can be used to estimate 3D pose of a human in different postures of a configurable bed. We explored two ConvNet architectures and found that both significantly outperformed data-driven baseline algorithms. Our kinematically embedded

ConvNet with link length regression provided a more complete representation of a 17-joint skeleton model, adhered to anthropomorphic constraints, and was able to adjust to participants of varying anatomy. We provided an example where joints on limbs raised from the pressure mat had a higher uncertainty than those in contact. We demonstrated our work using a PR2 robot.

### ACKNOWLEDGMENT

This material is based upon work supported by the National Science Foundation Graduate Research Fellowship Program under Grant No. DGE-1148903, NSF award IIS-1514258, NSF award DGE-1545287, and the National Institute on Disability, Independent Living, and Rehabilitation Research (NIDILRR), grant 90RE5016-01-00 via RERC TechSage. Any opinion, findings, and conclusions or recommendations expressed in this material are those of the author(s) and do not necessarily reflect the views of the National Science Foundation.

### REFERENCES

- [1] K. Hawkins, P. Grice, T. Chen, C.-H. King, and C. C. Kemp, “Assistive mobile manipulation for self-care tasks around the head,” in *2014 IEEE Symposium on Computational Intelligence in Robotic Rehabilitation and Assistive Technologies*. IEEE, 2014.
- [2] A. Kapusta, Y. Chitalia, D. Park, and C. C. Kemp, “Collaboration between a robotic bed and a mobile manipulator may improve physical assistance for people with disabilities,” in *RO-MAN*. IEEE, 2016.
- [3] P. M. Grice and C. C. Kemp, “Assistive mobile manipulation: Designing for operators with motor impairments,” in *RSS 2016 Workshop on Socially and Physically Assistive Robotics for Humanity*, 2016.
- [4] T. Harada, T. Mori, Y. Nishida, T. Yoshimi, and T. Sato, “Body parts positions and posture estimation system based on pressure distribution image,” in *ICRA*, vol. 2. IEEE, 1999, pp. 968–975.
- [5] J. J. Liu, M.-C. Huang, W. Xu, and M. Sarrafzadeh, “Bodypart localization for pressure ulcer prevention,” in *EMBC*. IEEE, 2014, pp. 766–769.
- [6] R. Grimm, S. Bauer, J. Sukkau, J. Hornegger, and G. Greiner, “Markerless estimation of patient orientation, posture and pose using range and pressure imaging,” *International journal of computer assisted radiology and surgery*, vol. 7, no. 6, pp. 921–929, 2012.
- [7] P. M. Grice, Y. Chitalia, M. Rich, H. M. Clever, and C. C. Kemp, “Autobed: Open hardware for accessible web-based control of an electric bed,” in *RESNA*, 2016.
- [8] Y. Gal and Z. Ghahramani, “Dropout as a bayesian approximation: Representing model uncertainty in deep learning,” in *Conference on Machine Learning*, 2016, pp. 1050 – 1059.
- [9] N. Sarafianos, B. Boteanu, C. Ionescu, and I. A. Kakadiaris, “3d human pose estimation: A review of the literature and analysis of covariates,” *Computer Vision and Image Understanding*, no. 152, pp. 1–20, 2016.
- [10] R. Okada and S. Soatto, “Relevant feature selection for human pose estimation and localization in cluttered images,” in *ECCV*. Springer, 2008, pp. 434–445.
- [11] C. Ionescu, D. Papava, V. Olaru, and C. Sminchisescu, “Human3.6m: Large scale datasets and predictive methods for 3d human sensing in natural environments,” *Trans. on Pattern Analysis and Machine Intelligence*, vol. 36, no. 7, pp. 1325–1339, 2014.
- [12] A. Agarwal and B. Triggs, “Recovering 3d human pose from monocular images,” *Pattern Analysis and Machine Intelligence, IEEE Transactions on*, vol. 28, no. 1, pp. 44–58, 2006.
- [13] A. Toshev and C. Szegedy, “DeepPose: Human pose estimation via deep neural networks,” in *CVPR*.
- [14] J. J. Tompson, A. Jain, Y. LeCun, and C. Bregler, “Joint training of a convolutional network and a graphical model for human pose estimation,” in *Advances in neural information processing systems*, 2014, pp. 1799–1807.
- [15] G. Pavlakos, X. Zhou, K. G. Derpanis, and K. Daniilidis, “Coarse-to-fine volumetric prediction for single-image 3d human pose,” in *CVPR*. IEEE, 2017.
- [16] X. Zhou, X. Sun, W. Zhang, S. Liang, and Y. Wei, “Deep kinematic pose regression,” in *ECCV 2016 Workshops*, 2016, pp. 186–201.
- [17] S. Li and A. B. Chan, “3d human pose estimation from monocular images with deep convolutional neural network,” in *Asian Conference on Computer Vision*. Springer, pp. 332–347.

- [18] R. V. Wei, Shih-En, T. Kanade, and Y. Sheikh, "Convolutional pose machines," in *CVPR*, 2016, pp. 4724–4732.
- [19] X. Zhou, M. Zhu, S. Leonardos, K. G. Derpanis, and K. Daniilidis, "Sparseness meets deepness: 3d human pose estimation from monocular video," in *CVPR*. IEEE, 2016, pp. 4966–4975.
- [20] F. Bogo, A. Kanazawa, C. Lassner, P. Gehler, J. Romero, and M. J. Black, "Keep it smpl: Automatic estimation of 3d human pose and shape from a single image," in *ECCV*. Springer, 2016, pp. 561–578.
- [21] T. Harada, T. Sato, and T. Mori, "Pressure distribution image based human motion tracking system using skeleton and surface integration model," in *ICRA*, vol. 4. IEEE, 2001, pp. 3201–3207.
- [22] R. Grimm, J. Sukkau, J. Hornegger, and G. Greiner, "Automatic patient pose estimation using pressure sensing mattresses," in *Bildverarbeitung für die Medizin 2011*. Springer, 2011, pp. 409–413.
- [23] M. Farshbaf, R. Yousefi, M. B. Pouyan, S. Ostadabbas, M. Nourani, and M. Pompeo, "Detecting high-risk regions for pressure ulcer risk assessment," in *BIBM*. IEEE, 2013, pp. 255–260.
- [24] S. Ostadabbas, M. B. Pouyan, M. Nourani, and N. Kehtarnavaz, "In-bed posture classification and limb identification," in *BioCAS*. IEEE, 2014, pp. 133–136.
- [25] A. Kendall and R. Cipolla, "Modelling uncertainty in deep learning for camera relocation," in *ICRA*. IEEE, 2016, pp. 4762–4769.
- [26] M. Kampffmeyer, A.-B. Salberg, and R. Jenssen, "Semantic segmentation of small objects and modeling of uncertainty in urban remote sensing images using deep convolutional neural networks," in *CVPRW*. IEEE, 2016, pp. 680–688.
- [27] D. Mehta, S. Sridhar, O. Sotnychenko, H. Rhodin, M. Shafiei, H.-P. Seidel, W. Xu, D. Casas, and C. Theobalt, "Vnect: Real-time 3d human pose estimation with a single rgb camera," *ACM Transactions on Graphics*, vol. 36, no. 4, pp. 44:1 – 44:14, 2017.
- [28] A. Paszke, S. Gross, S. Chintala, G. Chanan, E. Yang, Z. DeVito, Z. Lin, A. Desmaison, L. Antiga, and A. Lerer, "Automatic differentiation in pytorch," 2017.
- [29] N. Dalal and B. Triggs, "Histograms of oriented gradients for human detection," in *CVPR*, vol. 1. IEEE, 2005, pp. 886–893.
- [30] D. P. Kingma and J. Ba, "Adam: A method for stochastic optimization," 2014.